Vol. 18(4), pp. 84-105, October-December, 2023
DOI: 10.5897/IJPS2023.5035
Article Number: 8AD395771345
ISSN: 1992-1950

http://www.academicjournals.org/IJPS

ACADEMIC JOURNALS
expand your knowledge

International Journal of Physical Sciences

Full Length Research Paper

Hydrogeological assessment of groundwater resources within Isuikwuato and environ South Eastern Nigeria: Agenda for food agriculture and clean water policies

Joshua Chima CHIZOBA[1], Ayatu Ojonugwa USMAN[1]*, Chukwudi Chris EZEH[2], Ifeanyi Augustine CHINWUKO[3], George-Best AZUOKO[1], Obinna Chigoziem AKAKURU[4] and Kenneth Obinna IHEME[5]

[1]Department of Applied Geophysics, Alex Ekwueme Federal University, Ndufu-Alike, Ikwo, Ebonyi State, Nigeria.
[2]Department of Geology and Mining, Enugu State University of Science and Technology, Enugu, Nigeria.
[3]Department of Applied Geophysics, Nnamdi Azikiwe University, Awka, Anambra State, Nigeria.
[4]Department of Geology, Federal University of Technology, Owerri, Imo State, Nigeria.
[5]Department of Geology and Mineral Resource, University of Ilorin, Kwara State, Nigeria.

Received 29 May, 2023; Accepted 7 August, 2023

Groundwater resources of the Isuikwuato area, south eastern Nigeria, have been evaluated using integrated geophysical and hydrogeochemical techniques, to determine the quality and usability of the groundwater for domestic and agricultural purposes. Twenty Vertical Electrical Soundings (VES) physicochemical analyses were done. Depth to aquiferous unit varies from 38 to 148 m. The hydrogeochemical characterization shows that anion area, 85% of the total water sample in the area is Cl^- dominant, whereas 10% are HCO_3^- dominant and 5% of the sample had mixed dominant ionic specie. In the cation area, 75% of the total water samples had Ca^{2+} as their dominant ionic specie, while 25% of the samples had mixed dominant ionic specie. According to the Piper diagram, the region is in the geochemical zone 1 (Alkalines earth exceeds Akalines). The Durov plot demonstrates that there is ionic exchange occurring within the groundwater zone with a hydrogeochemical evolution trend of Cl^-> HCO_3^- +CO_3^{2-}> Ca^{2+}>Na^++K^+> SO_4^{2-}> Mg^{2+}. Principal Component Analysis (PCA) values indicated loadings were present for 37.42% of the parameters (PP) in PP1, 65.60% of the parameters in PP2 and in PP3, it had 75.23 loadings. The water is suitable for agriculture giving the value of calculated Sodium Adsorption Ratio (SAR) that ranges from 0.20 – 0.56. This study recommends that the government should leverage this to availability of clean water and food to the people to enable it to achieve its sustainable development goals (SDGs).

Key words: Groundwater, hydrogeochemistry, geophysical, aquiferous zone, Isuikwuato.

INTRODUCTION

Water is one of the most important resources on planet Earth, although its existence is a mystery to man. Groundwater occurs within the subsurface and dissolves mineral, ores and crude as they percolate inside the subsurface. There is a great relationship between geology and the chemistry of groundwater (Aikpokpodion et al., 2010; Yuan et al., 2014).

Considerable effort may be required in some situations

to locate suitable borehole sites. In other to achieve this, there is a need to understand the subsurface geology, stratigraphy and the hydrogeology of the area, and apply the necessary geophysical techniques. Boreholes have usually been drug with or without earlier information of the underlining geology; this has led to borehole failure (Anizoba et al., 2015). Isuikwuato and its surrounding areas have experienced a significant surge in infrastructural development and population growth. Consequently, there has been a substantial increase in the demand for potable water for human consumption and agricultural use. Therefore, it is imperative to assess the quality of groundwater from boreholes in the study area to determine its suitability for domestic and agricultural purposes. Given that surface water sources in the area are insufficient to meet this demand, there is a heightened focus on utilizing groundwater. Groundwater is found in saturated zones beneath the land surface. Additionally, many unsuccessful boreholes have been reported in the Isuikwuato area, and the quality of functioning boreholes for groundwater supply remains unknown. The presence of groundwater quality issues in the area will have negative implications due to the growing reliance on groundwater supply by the increasing population. Therefore, it is of utmost importance to evaluate the groundwater potential in the area for domestic and agricultural use (Usman et al., 2022). Tremendous breakthroughs have been recorded in the use of electrical methods in the exploration of subsurface water (Selemo et al., 1995). Also, the geophysical method using the Schlumberger technique is an effective tool for ascertaining the subsurface geologic configuration and stratification (Davis and Deweist 1966; Anizoba et al., 2015; Gopinath et al., 2018). Also, the geophysical method using the Schlumberger technique is an effective tool for ascertaining the subsurface geologic configuration and stratification (Anizoba et al., 2015; Gopinath et al., 2018).

It is worth noting that the quality of water is a function that depends on its usage (Anudu et al., 2008; Egboka, 1986). The primary uses of water are mainly for domestic activities like; drinking, cooking, bathing and general cleanliness such as washing and for agricultural purposes such as irrigation and livestock farming. It is necessary to consider the quality and quantity of water supply to improve the socially, economic and agricultural undertakings of man. The geophysical method for groundwater exploration is a modern tool which obtains information about the earth's electrical resistivities which help in characterizing the underlining rocks via their water content holding capacity (Akakuru et al., 2017).

Physicochemical study the spread, association and mobility of elements in groundwater to construe and reconstruct the geochemical processes in the environment (Chukwu, 2008). Earlier works reveal that solutes show the physicochemical background settings of a research area, and are predisposed by both human activities and nature (Chetelat et al., 2008; Gopinath et al., 2016; Zhu et al., 2019).

Knowledge of groundwater potential vis-à-vis the hydro-geophysical and physiochemical investigation in the area is of fundamental importance since there have been cases of failed boreholes, to reduce well failure, thereby increasing precision and result oriented groundwater resources management programs in the area. It is anticipated that the result of the research will be useful material on the use of groundwater by both domestic and agricultural proposes. It can also serve as a background document for groundwater resources within and outside the research area.

Geology and hydrogeology

The research area lies between latitudes 05042'0''N and 05050'30''N and longitudes 7023'0''E and 7033'0''E (Figure 1). The area is underlain by a succession of geologic units which include: The Nsukka Formation, Ajali Formation, Mamu Formation and Nkporo Formation (Figure 2). The Nsukka Formation which is Danian in age has Nadu River as a type locality which is about 14 km north of Nsukka. Lithologically it comprises an interchanging sequence of sandstone, dirty shale and thin coal seam intercalated with sand at various layers (Chukwu, 2008; Reyment, 1965; Obi et al., 2001). The base of the Nsukka formation consists of thick sandstone. The Ajali Sandstone is of upper Maastrichtian. Its lithology consists of poorly sorted, friable sandstones (Obi et al., 2001). Underlining the Ajali sandstone formation is the Mamu Formation, chronologically, it is Maastrichtian/Upper Santonian. Lithologically, it comprises well-defined build-ups of sandstone, mudstone, shale, and sandy shale, with intercalated coal seams. Additionally, it contains fine-bedded, fine-to-medium sandstones that are white or yellow (Chukwu, 2008; Emmanuel and Nurudeen, 2012). Reyment (1965) has described the Nkporo Shales as consisting of dark shales and mudstones with subordinate sandstone and limestone.

The high precipitation in the research area offers sufficient recharge for the aquifers. The Northeastern part of the researched area, which the Nkporo Formation

*Corresponding author. E-mail: ayatu.ao@funai.edu.ng

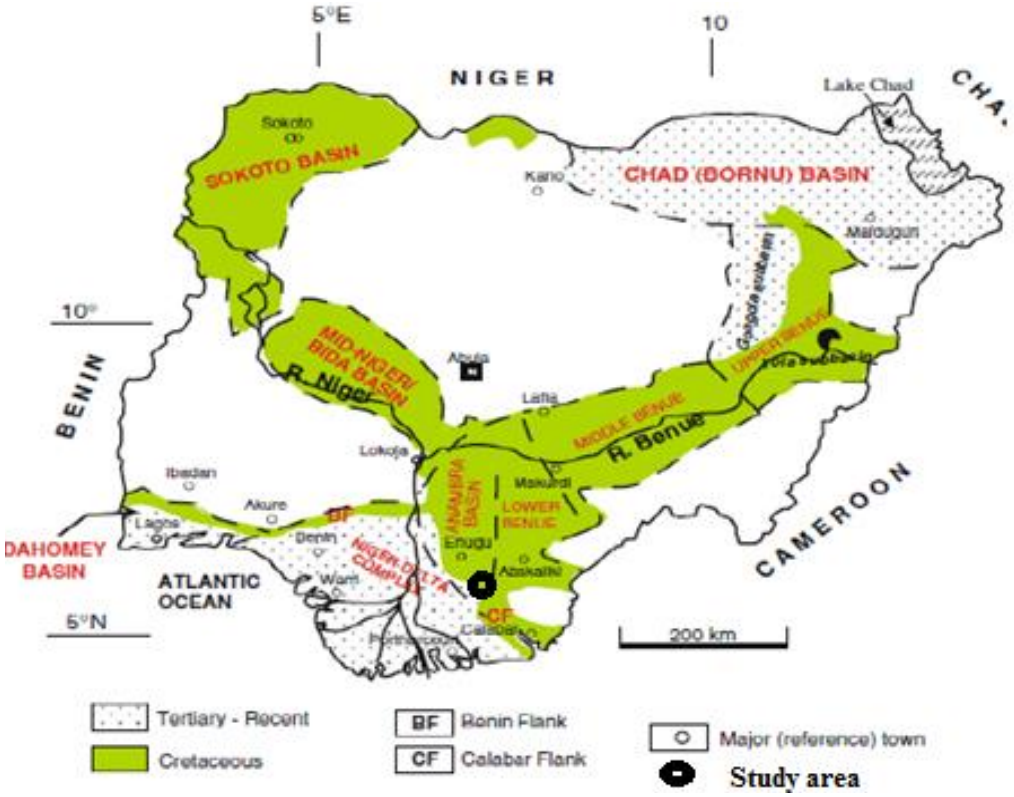

Figure 1. Geologic Map of Nigeria showing the study area.

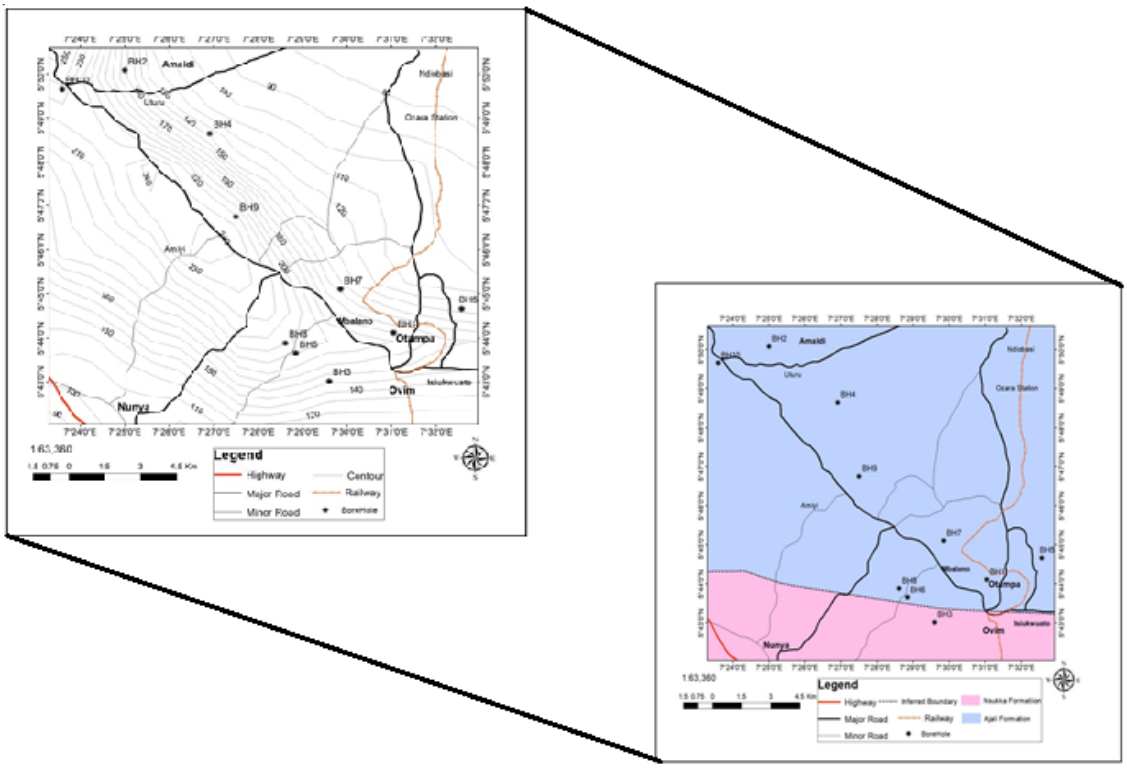

Figure 2. Location and Geology map of the research area.

Table 1. The global grid positions and VES locations obtained during the fieldwork using the GPS receiver.

Profile number	VES location	Latitude	Longitude	Elevation (m)
VES 1	EziamaNunya	$5^0$42.503^{l}N	$7^0$24.628^{l}E	110
VES 2	AmacharaAcha	$5^0$49.128^{l}N	$7^0$30.512^{l}E	81
VES 3	Amaibo	$5^0$46.152^{l}N	$7^0$29.826^{l}E	116
VES 4	Pharmaceutical Science ABSU	$5^0$49.526^{l}N	$7^0$23.509^{l}E	170
VES 5	NdiOgu-Eluama	$5^0$45.103^{l}N	$7^0$25.723^{l}E	201
VES 6	AmabaOvim	$5^0$43.723^{l}N	$7^0$30.859^{l}E	190
VES 7	UmuamaEluama	$5^0$44.594^{l}N	$7^0$27.749^{l}E	235
VES 8	Amagu – Uturu	$5^0$50.198^{l}N	$7^0$24.834^{l}E	172
VES 9	General teaching hospital Isuikwato	$5^0$43.972^{l}N	$7^0$30.303^{l}E	223
VES 10	Amawo	$5^0$46.761^{l}N	$7^0$27.109^{l}E	194
VES 11	Umuobiala	$5^0$43.204^{l}N	$7^0$28.276^{l}E	192
VES 12	OgwahiaUturu	$5^0$49.947^{l}N	$7^0$25.277^{l}E	114
VES 13	AmaukoUturu	$5^0$48.883^{l}N	$7^0$26.337^{l}E	127
VES 14	UgwuntaOvim	$5^0$44.297^{l}N	$7^0$32.347^{l}E	177
VES 15	UmuebereajaEluama	$5^0$43.887|N	$7^0$27.602^{l}E	176
VES 16	Ndi Oro AmiyiUhu	$5^0$45.386^{l}N	$7^0$29.491^{l}E	174
VES 17	ObunaebereNkumeEluama	$5^0$43.777^{l}N	$7^0$26.462^{l}E	177
VES 18	AmokweAmaba	$5^0$43.796^{l}N	$7^0$31.308^{l}E	210
VES 19	UmuebereNkume	$5^0$43.525^{l}N	$7^0$26.563^{l}E	157
VES 20	ABSU Junction	$5^0$50.000^{l}N	$7^0$23.490^{l}E	267

underlined, has smaller groundwater potential. The Ajali Formation towards Ndi-Ogu Eluama, Umuobiala and Umuama is highly permeable, dominated by sand and has weathered top of higher groundwater availability when compared to the other Formations here. Also, shales of the Nsukka Formation provide aquiferous units because of the secondary porosity established by the intrusion deed developing linear fractures and cross-cutting (Chukwu, 2008).

STUDY METHODS

Resistivity survey

Vertical Electrical Sounding (VES) using Schlumberger configuration is one of the reliable electrical resistivity techniques in hydro-geophysical studies. The Global positioning system (GPS) positions and VES locations are shown in Table 1.

Fundamentally, four electrodes (two current electrodes (AB) and two potential electrodes (MN)) and a resistivity meter were placed as shown in Figure 3 during the survey. The survey was done by increasing the current electrode spacing which implies increment and recording the corresponding resistivity values at each depth of investigation. The apparent resistivity () is computed as guided by Equations 1 and 2 (Adetola and Igbedi, 2000; Ezeh et al., 2022; Omali et al., 2000);

$$AM = BN \frac{a-b}{2} \; and \; BM = \frac{a+b}{2} \quad (1)$$

$$\rho_a = \pi \left(\frac{a^2}{b} - \frac{b}{4}\right)\frac{\Delta V}{I} \text{ Or } \rho_a = GR \quad (2)$$

Where, ρ_a = apparent resistivity, G = the geometric factor, R = resistance, V = potential difference.

Collection/physicochemical analyses

Ten borehole water samples were collected in different communities of the researched area. Most boreholes sampled are situated mainly within a sedimentary formation in the district. Physicochemical analysis was carried out mainly to evaluate the groundwater quality of the area. Two litres of water samples were collected in clean plastic containers already rinsed with the same water to be sampled. Two water samples were collected at each location. Preceding the sample collection, the boreholes were pumped for a minimum of five minutes to guarantee the collection of a representative sample. Samples were collected and labeled in plastic polyethylene bottle containers tightly corked. The choice of plastic containers is to ensure minimal contamination. The samples were taken to the laboratory for analysis within 24 h.

The determination of the physicochemical properties of the water samples was carried out by established standard methods. These properties encompassed Temperature, pH, Electrical conductivity, Total Dissolved Solids (TDS), Total Suspended Solids (TSS), Total Solids (TS), Turbidity, Total hardness, Dissolved Oxygen (DO), Total alkalinity, Cations (Magnesium, calcium, potassium, sodium), Anions (bicarbonate, nitrates, sulphates, chlorides), and Trace metals (manganese, iron).

Measurements of temperature were conducted using mercury in a glass thermometer. The conductivity of the samples was determined utilizing a conductivity meter, with the probe being immersed in the sample container until a consistent reading was obtained and recorded. The pH value was determined through the use of a pH Meter, specifically the PBS–51 model from EL–Hama instrument. Turbidity, on the other hand, was determined utilizing a

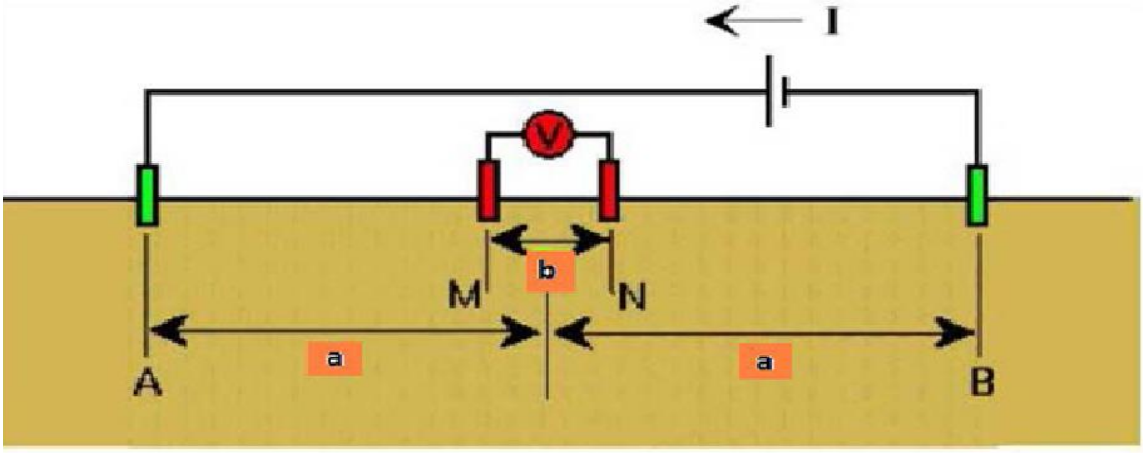

Figure 3. Diagrammatic representation of Schlumberger array (Chinwuko et al., 2015; 2016).

standardized Hanna H198703 Turbidimeter. As for the Cations (Ca2+, Mg2+, K+, Na+, Fe2+, and Mn2+), 100 cm3 of the water sample underwent pre-concentration through vacuum heating until a reduction to 25cm3 occurred. Determination of these Cations was then performed using the Atomic Absorption Spectrophotometer (AAS). The Anions (SO42-, HCO3-, Cl-, and NO3-), on the other hand, were determined utilizing the digital titration method.

Statistical background

The generated datasets underwent analysis using summary and descriptive statistics, such as average, range, and standard deviation, to compare them against recommended standards for drinking water. Several models, including the Piper diagram, Durov diagram, and Scholler diagram, were employed for the identification of hydrogeochemical facies and the determination of the dominant ions influencing groundwater chemistry in the area. The Piper diagram, established by Piper (1944), is a renowned method for categorizing water samples based on groundwater facies and other criteria, illustrating the relative abundance of common ions. Additionally, the Durov diagram, a hydrogeological visualization technique, presents major ion percentages in milli-equivalents through two trilinear graphs that form additional two-dimensional projections. Furthermore, the application of multivariate statistics involved the utilization of the correlation matrix and Principal Component Analysis, by the research conducted by Akakuru et al. (2023).

RESULTS AND DISCUSSION

Geophysical results and discussions: Interpretations of VES results

Twenty VES sounding was done within the selected communities and computed using the *IPI2 WIN* software package (Bobachev, 2002; Usman et al., 2015). Hence, apparent resistivity (ρ_a) (on the Y axis) was plotted against half current electrode spacing (on the X axis).

VES results

The field curves generated by the interpreted VES data are shown in Figures 4 to 7. While the summary of VES data interpretation and geoelectric section were shown in Table 2 and Figures 4 to 7 respectively. Figure 8 shows the interpreted geoelectric section result interpreted from the curve.

The results geoelectric sections (Figure 10 and Table 2) of the various VES stations in the researched area were created to show the various lithologic layers; thicknesses within the depths penetrated and characteristic resistivity values. The profiles were taken along the AA1, BB1, CC1, DD1 and EE1 directions (Figure 9). The geoelectric section AA1 that passes across the NW-SE direction of the researched area cut cross VES 3, 8, 12, 13 and 14 (Figure 10). The interpretative cross-section of AA1 shows three to five geoelectric layers. The first layer has a resistivity value ranging from 174 to 718 Ω.m with a thickness that varies from 0.6 to 8.9 m and is composed of predominantly top sandy soil. Underlining the first layer is a shale unit with resistivity values that vary from 9.2 to 5310 Ω.m in VES 3 and sand in other VES locations. The third layer with resistivity range of 13.1 to 718 Ω.m and a thickness between 12.8 and 66.1 m.

The base bottom was not reached and has a resistivity value range of 15.1 to 1980 Ω.m. It was interpreted as water shale. The interpretive geoelectric section of BB1 across the southeast-northwest direction is made up of ata from VES 6, 9, 10, 16 and 18 (Figure 10). The geoelectric sections also show four to five geoelectric layers. The sections have resistivity values ranging from 133 to 487 Ω.m and are characteristic of topsoil in the southeastern part and weathered shale at VES 16.

Beneath the topsoil layer towards the southeastern part,

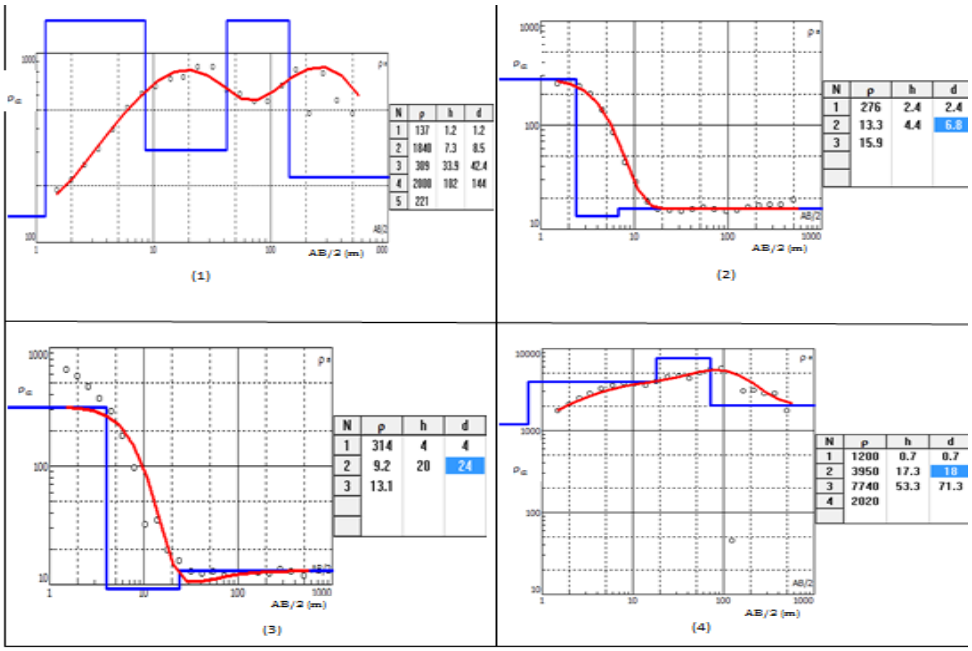

Figure 4. VES 1, 2, 3 and 4 curves.

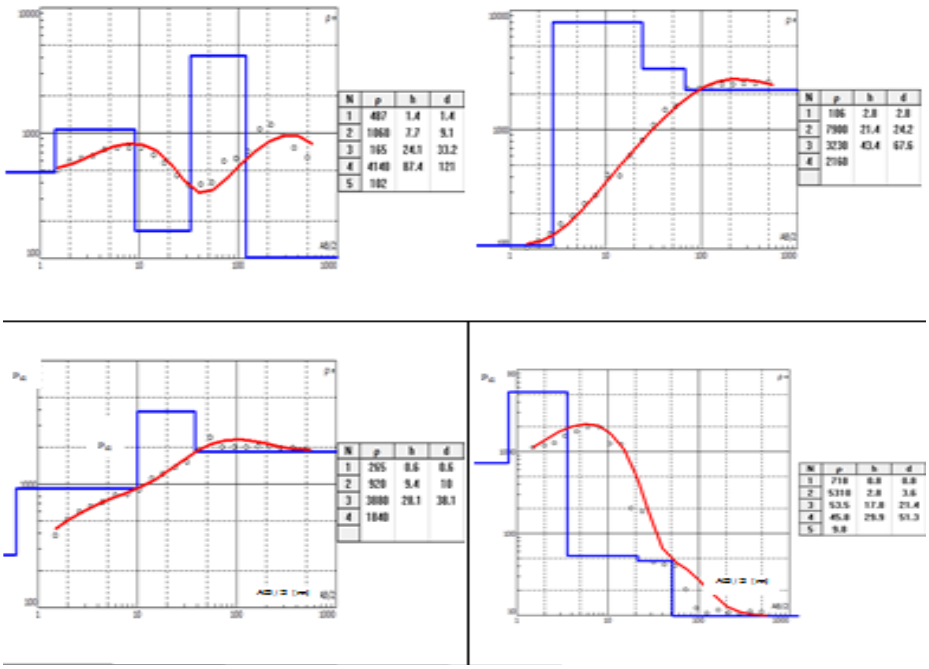

Figure 5. VES 5, 6, 7 and 8 curves.

lateritic sand with a relative resistivity range of 17.9 to 7900 Ω.m was observed under the top soil which does not extend to VES 10 and 14 is characteristic of lateritic sand. It is followed by a third layer with a resistivity range of 76 to 8100 Ω.m and thickness between 22.3 and 96.6 m. The next unit with resistivity values ranging from 7.6 to

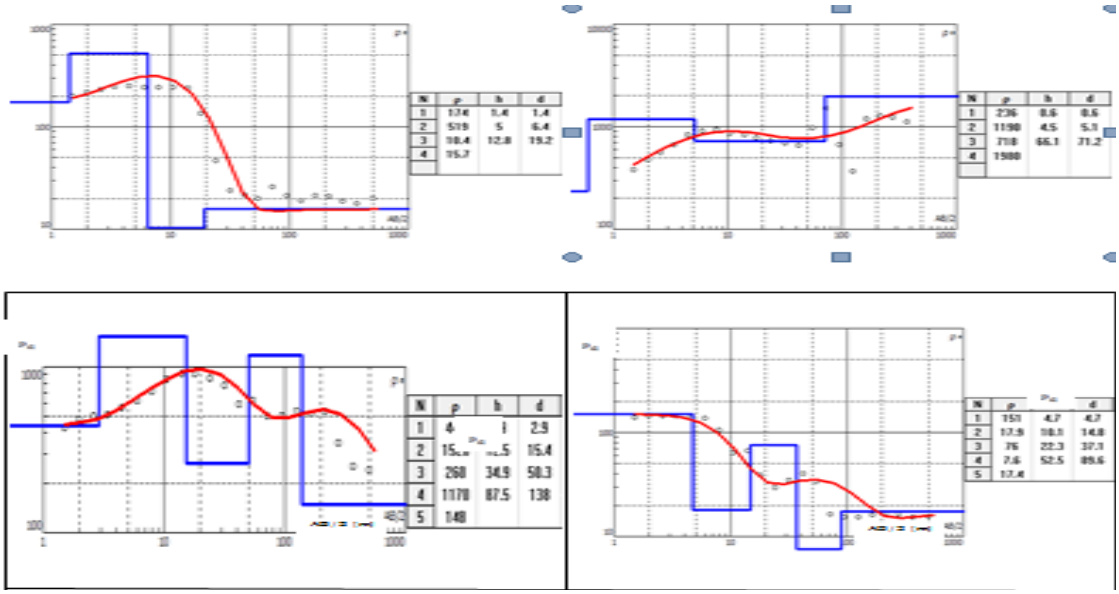

Figure 6. VES 9, 10, 11 and 12 curves.

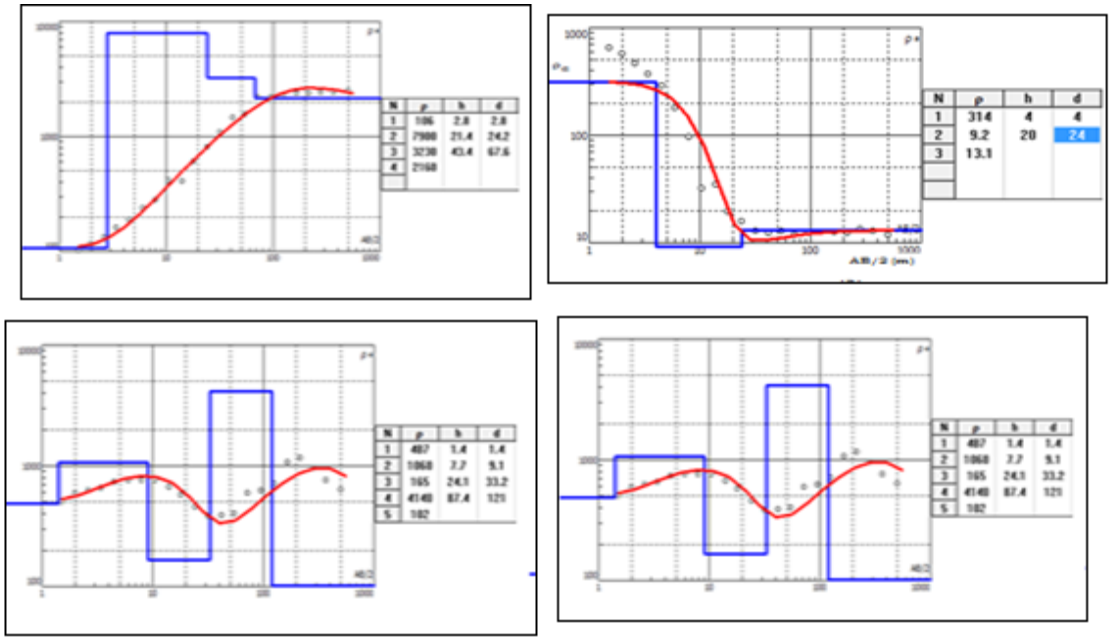

Figure 7. VES 13, 14, 15 and 16 curves.

4140 Ω.m is presumed to be saturated sandstone in VES 6, 10 and 18, and identified as dry sandstone at VES 9 and shale at VES 16. The basal unit at VES 9 is the saturated sandstone and shale at VES 16.

The geoelectric section across the CC1 profile is made up of data from VES 4, 7, 11, 15 and 20. The geoelectric section shows four to five geoelectric layers. The topsoil has a resistivity value ranging from 202 to 5020 Ω.m with thickness varying from 0.6 to 2.9 m characteristic of top sandy soil. Beneath the topsoil is the lateritic sand, with a resistivity range of 920 to 3420 Ω.m. This is underlain by dry sand with a resistivity range between 260 and 28500 Ω.m and a thickness range of 28.1 to 66.4 m. The basal layer whose bottom was not reached in VES 4, 7, 11 and

Table 2. Summary of geoelectric results.

VES point	Layer	Resistivity(Ωm)	Thickness(m)	Depth(m)	Inferred lithology
1	1	137	1.2	1.2	Top soil
	2	1840	7.3	8.5	Dry sand
	3	309	33.9	42.4	Silty sand
	4	2000	102	144	Sandstone
	5	221	∞	∞	Saturated sand
2	1	276	2.4	2.4	Top silty soil
	2	13.3	4.4	6.8	Weathered shale
	3	15.9	∞	∞	Shale
3	1	314	4	4	Top silty soil
	2	9.2	20	24	Silty shale
	3	13.1	∞	∞	Shale
4	1	1200	0.7	0.7	Top sandy soil
	2	3950	17.3	18	Lateritic sand
	3	7740	53.3	71.3	Dry sand
	4	2020	∞	∞	Saturated sand
5	1	1110	3.5	3.5	Top soil
	2	23800	7.7	11.2	Dry sand
	3	16500	23.3	34.5	Hard sand
	4	4340	54.3	88.5	Wet sandstone
	5	3900	∞	∞	Saturated sand
6	1	196	0.7	0.7	Top soil
	2	840	9.9	10.6	Lateritic soil
	3	340	60.4	71	wet sand
	4	1200	∞	∞	Saturated sand
7	1	202	0.6	0.6	Top silty soil
	2	970	16.2	16.8	Lateritic sand
	3	28500	66.4	83.2	Dry sandstine
	4	3490	∞	∞	Saturated sand
8	1	400	8.9	8.9	Top soil
	2	126	20.4	29.3	wet sand
	3	106	27.9	57.2	shaly mudstone
	4	15.1	∞	∞	Shale
9	1	487	1.4	1.4	Top sandy soil
	2	1060	7.7	9.1	wet sand
	3	165	24.1	33.2	silty sandstine
	4	4140	87.4	121	Dry sandsand
	5	102	∞	∞	saturated sand
10	1	106	2.8	2.8	Top soil
	2	7900	21.4	24.4	Dry sand
	3	3230	43.4	67.6	wet sand

Table 2. Cont'd

	4	2160	∞	∞	Saturated sand
11	1	265	0.6	0.6	Top soil
	2	920	9.4	10	Lateritic soil
	3	3880	28.1	38.1	Dry sand
	4	1840	∞	∞	Saturated sand
12	1	718	0.8	0.8	Top sandy soil
	2	5310	2.8	3.6	Sandstone
	3	53.5	17.8	21.4	Hard sand
	4	45.8	29.9	51.3	Weathered shale
	5	9.8	∞	∞	Shale
13	1	174	1.4	1.4	Top soil
	2	519	5	6.4	Lateritic sand
	3	10.4	12.8	19.2	shaly mudstone
	4	15.7	∞	∞	Shale
14	1	236	0.6	0.6	Top soil
	2	1190	4.5	5.1	Dry sand
	3	718	66.1	71.2	Sandstone
	4	1980	∞	∞	Shaly sandstone
15	1	444	2.9	2.9	Top soil
	2	1520	12.5	15.4	Lateritic soil
	3	260	34.9	50.3	Wet sand
	4	1170	87.5	138	Hard sand
	5	148	∞	∞	Saturated sand
16	1	151	4.7	4.7	Weathered shale
	2	17.9	10.1	14.8	Mudy shale
	3	76	22.3	37.1	shaly mudstone
	4	7.6	52.5	89.6	silty shale
	5	17.4	∞	∞	Shale
17	1	271	0.7	0.7	Hard ironstone
	2	1470	8.4	9.1	Lateritic sand
	3	191	29.7	38.8	Silty sand
	4	1270	47.2	86	wet sand
	5	5730	∞	∞	Saturated sand
18	1	133	1.4	1.4	Top soil
	2	1020	24.8	26.3	Lateritic soil
	3	8100	96.6	123	Dry sand
	4	2590	∞	∞	Saturated sand
19	1	890	0.7	0.7	Top soil
	2	1170	17.5	18.2	Stony laterite
	3	3840	41.4	59.6	Silty sand

Table 2. Cont'd

	4	2090	88.4	148	wet sand
	5	5240	∞	∞	Saturated sand
20	1	5020	1.8	1.8	Top soil
	2	3420	21.5	23.3	Lateritic sand
	3	19300	86.1	109	Dry sand
	4	5090	∞	∞	Saturated sand

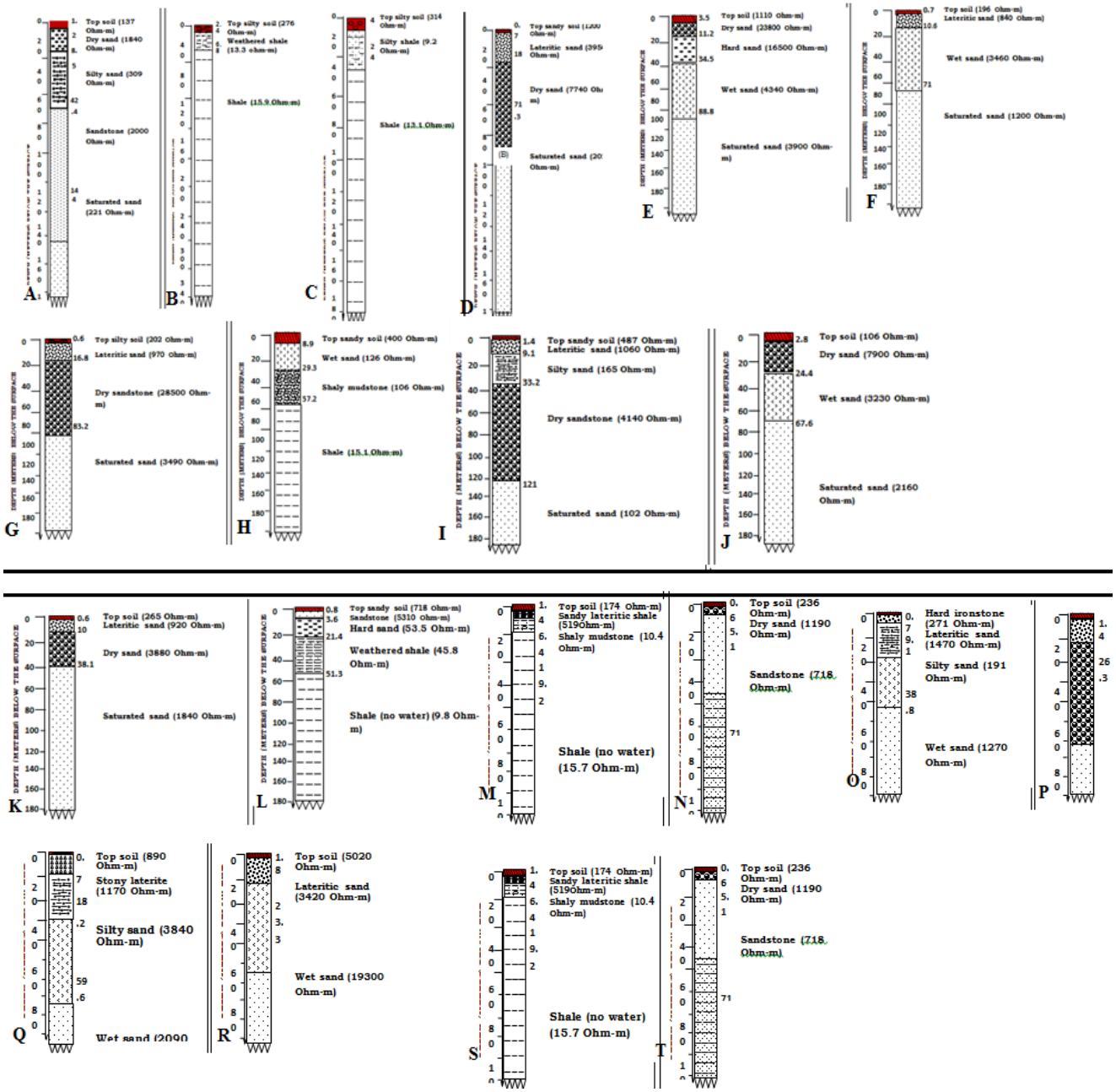

Figure 8. Geoelectric section VES 1-VES 20.

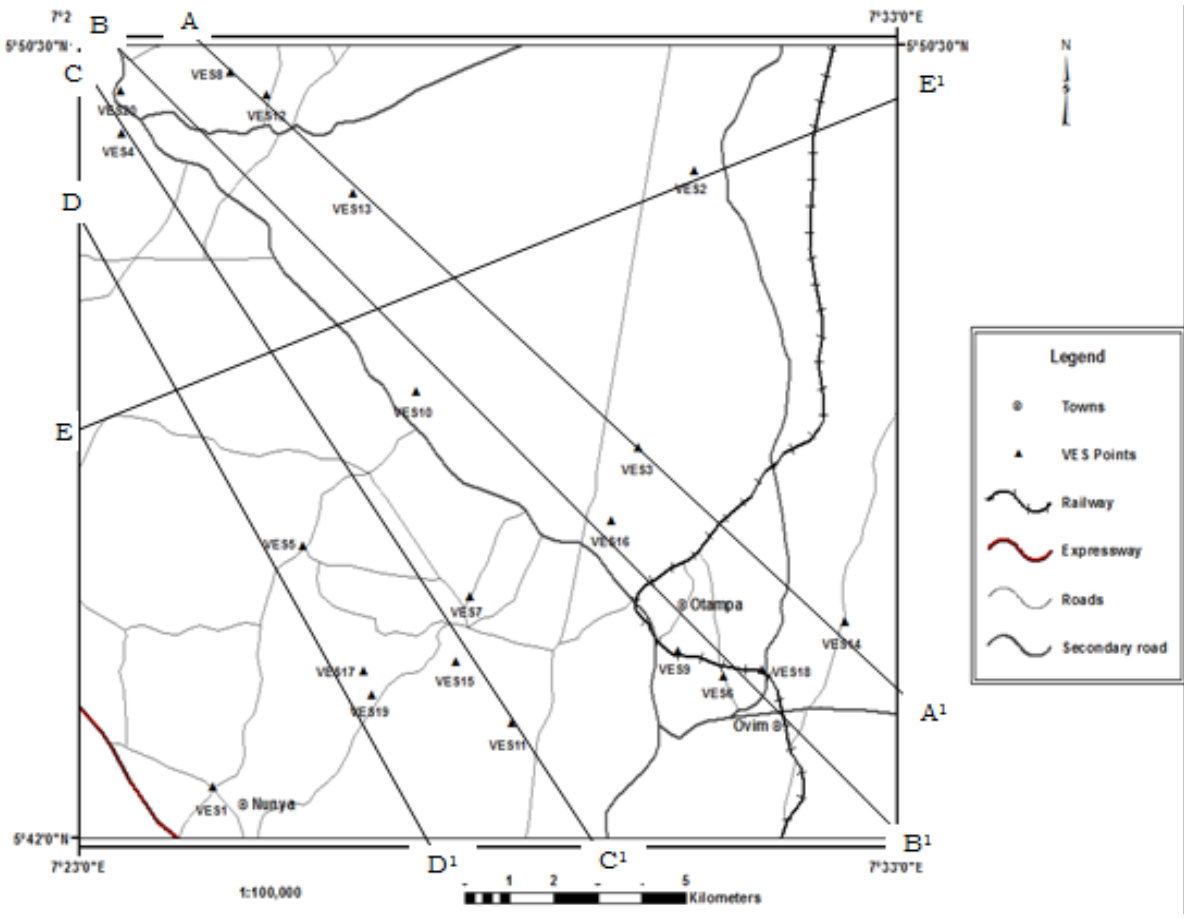

Figure 9. Accessibility map of the study area showing VES points and various profiles.

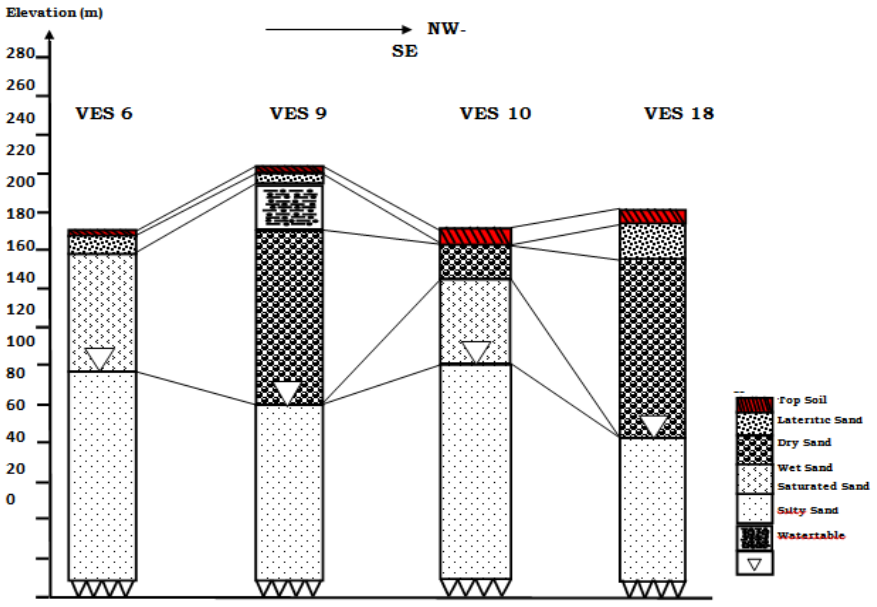

Figure 10. Geoelectric correlations of profile CC^1 and BB^1 cross-section taken along the northwest- southeast direction of the area of study.

20 has resistivity values between 1840 to 5090 Ω.m. It was interpreted as water-saturated sandstone which is the prospective aquifer unit of interest. Although saturated sandstone in VES 15 is in the fifth layer. The geoelectric section across the DD1 profile is composed of five geoelectric layers in the study area. The geoelectric section is made up of VES 1, 5, 17 and 19. The topsoil thickness is relatively thin along this profile and ranges between 0.7 and 3.5 m while the resistivity values range between 137 and 1110 Ω.m. The next layer has a resistivity value range of 1170 to 23800 Ω.m and a thickness range of 7.3 to 17.5 m. The third layer which varies in resistivity from 191 to 16500 Ω.m with thickness values that varies from 23.3 to 41.4 m has a predominant composition of silty sand. The underlying layer is interpreted as wet sand with resistivity values ranging from 1270 to 4340 Ω.m. The basal layer whose depth was not reached has a resistivity value between 221 and 5730 Ω.m. It was interpreted as water-saturated sandstone which is the prospective aquifer unit of interest. Three horizons were delineated in VES 2 from the EE1 profile. The first layer has a resistivity value of 276 Ω.m and a depth of 2.4 m. This layer is the topsoil. The next layer has a lower resistivity value of 13.3 Ω.m. This layer is interpreted to be weathered shale with a thickness of 4.4 m. The last layer is interpreted as shale with a low resistivity value of 15.9 Ω.m, though the base was not reached.

A profile along BB1 and CC1 was taken across the NW-SE flank of the study area to determine the comparative correlation within the researched area using geoelectric sections. The correlation of geoelectric sections along CC1 was modelled (Figure 10) and it reveals that the thickness of laterite within VES 20 is higher when compared with that of VES 4, 7, 11 and 15. The water table is shallower at VES 11 and VES 4 with depth to water table occurring at 38.1 to 71.3m, while VES 7, 15 and 20 with depth to water table ranges from 83.2 to 138 m are the deepest part. The lithologic facies are top soil, lateritic sand, dry sand, wet sand and saturated sand. Hence, the depth auriferous unit is continuous within this area, and the aquifer units in the area are capable of yielding good water for human use. Meanwhile, the correlation along BB1 in the NW-SE direction (Figure 10) shows the high thickness of topsoil at VES 10. The deepest depth to a saturated unit within this region is at VES 18 (Amokwe Amaba), whereas VES 6, 9 and 10 have shallower saturated units. The auriferous layers are unremitting with several lithology changes around the researched area and can produce an optimum amount of water.

Maps of the apparent resistivity and depth were prepared using interpreted VES results. The map of resistivity variation is shown in Figure 11, while the 2-D and 3-D depth maps are shown in Figures 12 and 13. Similarly, the 2-D and 3-D water-table depth maps in Figures 11 and 13 show the distribution of the depth to water-table computed from the VES results. The water table depth is higher towards the Southern part of the researched area, thus, high prospect for groundwater towards this area. The VES location is shown in Figure 9.

Physicochemical results

The results of the physicochemical analysis are shown in Table 3. Low pH of the water (more acidic) may lead to metal corrosion. The pH values gotten ranged from 3.9 to 7.8. 40% of the total samples are within the World Health Organization (WHO) permissible limit for potable water, except a few samples that have pH values below the WHO neutral value (pH 7) as the acceptable pH for drinking water is between 6.50 and 8.50 as shown in Table 4 (WHO, 2006). The result was compared favourably with the report by Akakuru et al. (2022), Anudu et al. (2008). The electrical conductivity (EC) value shows the acceptable limit of 500 µS/cm given by the WHO for the entire borehole sample. EC is a pointer of soil saline content and water quality, therefore the equitably low values analyzed in some water samples suggest low saline content; therefore, the waters are adequate for domestic and agricultural usage. These values obtained are similar to those reported values by Anudu et al. (2008) and WHO/UNEP/UNESCO/WMO 1998. Total dissolved solids (TDS) values were in the range of 25.95 to 56.65 mg/L, it contains inorganic salts (mainly calcium (Ca), magnesium (Mg), potassium (K), sodium (Na), trioxocarbonate (HCO3), chlorine (Cl) and sulphur (S)) and little quantity of organic matter dissolved in water. The TDS values are predominately below 500 mg/L which falls within the WHO permissible limit for potable water. The sample from borehole 5 had the highest TDS while the sample from borehole 8 had the least. It was detected that an increase in EC resulted in increasing TDS. These results compare favourably with the works of Iheme et al. (2018b) and Udoh et al. (2021).
DO, sample 8 has the maximum concentration. The DO values range from 7.15 to 7.98 mg/L, and most of the samples DO are below the WHO permissible limit, except for a few samples with DO values slightly above WHO acceptable limit. Chlorides in drinking water are mostly from natural sources, industrial wastes and sewage. Salinity (Cl^-) is a major anion in water, and excess of it might cause edema (swelling of plant organs or parts). The result gotten for chloride ranges from 6.2 to 24.11 mg/L. These ranges of values are below the acceptable value of 200 mg/L by the WHO and by Emmanuel and Nurudeen (2012). Also, the factor measured for the appropriateness of water for livestock farming is total dissolved solids. The Australian standards for livestock water (Hamill and Bell, 198l, 2016), we concluded that the water is appropriate for livestock farming with TDS

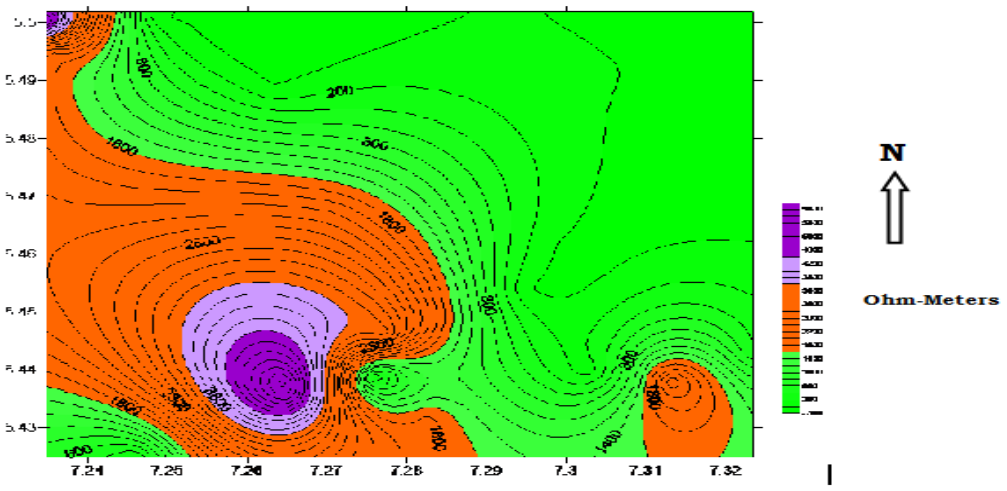

Figure 11. Resistivity map of the study area.

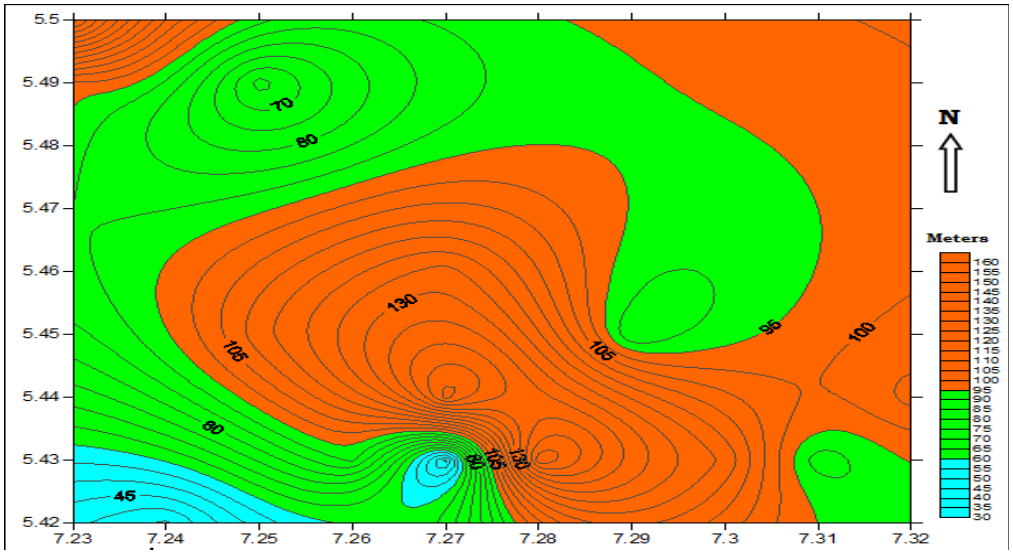

Figure 12. The water table depth map.

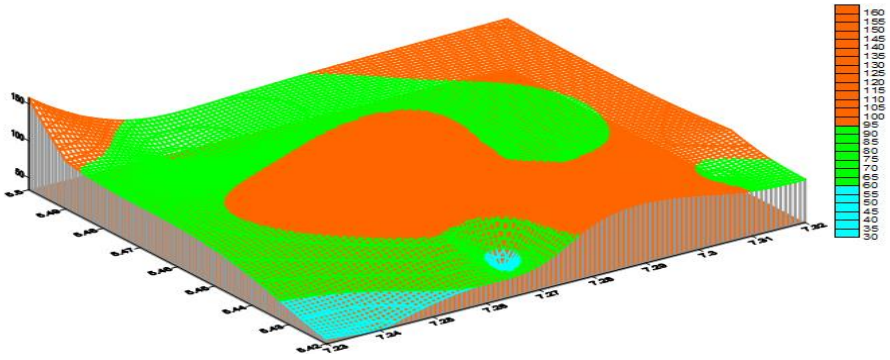

Figure 13. 3-D Wireframe water table depth map of the study area.

Table 3. Results of physicochemical characteristics of groundwater in Isuikwuato.

Parameter	pH	Ec,µS/cm	TDS (mg/L)	Ca, (mg/L)	Mg (mg/L)	Cl (mg/L)	SO_4 (mg/L)	NO_3 (mg/L)	DO (mg/L)	K (mg/L)	Na (mg/L)	Fe (mg/L)	HCO_3 (mg/L)
BH1	5.1	84.3	54.8	6	0.6	19.85	6.03	4.08	7.86	3.2	4.8	0.01	18
BH2	7.4	59.93	38.95	7.6	0.6	19.85	0.47	3.31	7.2	1.3	2.14	0.01	21
BH3	5.7	81.96	53.27	6	0.6	18.43	3.11	2.23	7.64	2.4	3.75	0.01	17
BH4	7.6	65.15	42.35	8.4	0.6	22.69	0.58	4.42	7.35	1.4	3.02	0.02	21
BH5	5.9	87.12	56.65	5.2	0.6	7	2.01	1.8	7.15	0.1	5.01	0.02	17
BH6	5.4	78.5	51.3	5.6	0.6	7.4	4.27	2.4	7.59	0.5	3.18	0.02	15
BH7	7.8	63.8	41	8.8	0.9	6.2	1.82	6.4	7.42	0.4	3.85	0.03	27
BH8	5.7	39.9	25.95	6	0.6	21.98	0.95	1.1	7.98	1.8	2.2	0.03	14
BH9	3.9	45.3	29.45	3.6	0.3	16.31	1.2	8.4	7.95	2.5	2.3	0.01	11
BH10	7.2	58.6	38.9	8.4	0.9	24.11	0.67	5.6	7.78	1.5	2.9	0.02	26
BH11	5.1	84.3	54.8	6	0.6	19.85	6.03	4.08	7.86	3.2	4.8	0.01	18
BH12	7.4	59.93	38.95	7.6	0.6	19.85	0.47	3.31	7.2	1.3	2.14	0.01	21
BH13	5.7	81.96	53.27	6	0.6	18.43	3.11	2.23	7.64	2.4	3.75	0.01	17
BH14	7.6	65.15	42.35	8.4	0.6	22.69	0.58	4.42	7.35	1.4	3.02	0.02	21
BH15	5.9	87.12	56.65	5.2	0.6	7	2.01	1.8	7.15	0.1	5.01	0.02	17
BH16	5.4	78.5	51.3	5.6	0.6	7.4	4.27	2.4	7.59	0.5	3.18	0.02	15
BH17	3.9	45.3	29.45	3.6	0.3	16.31	1.2	8.4	7.95	2.5	2.3	0.02	11
BH18	7.2	58.6	38.9	8.4	0.9	24.11	0.67	5.6	7.78	1.5	2.9	0.02	26
BH19	5.1	84.3	54.8	6	0.6	19.85	6.03	4.08	7.86	3.2	4.8	0.01	18
BH20	7.4	59.93	38.95	7.6	0.6	19.85	0.47	3.31	7.2	1.3	2.14	0.01	21
Mean	6.12	68.48	44.60	6.50	0.62	16.96	2.30	3.97	7.58	1.63	3.36	0.02	18.60
Min	3.90	39.90	25.95	3.60	0.30	6.20	0.47	1.10	7.15	0.10	2.14	0.01	11.00
Max	7.80	87.12	56.65	8.80	0.90	24.11	6.03	8.40	7.98	3.20	5.01	0.03	27.00

<100 mg/L. Hence, the plot of the borehole samples analytical on the US salinity diagrams (Richards, 1954) shows that most of the analyzed samples are within the acceptable field of C1S1, under low salinity and low Na hazard (Figure 14). This reaffirms the outstanding nature of the water for irrigation purposes irrespective of the soil and without exchangeable Na danger. Also, it compares favourably with the reports by Paschal et al. (2014), Anudu et al. (2008) and Usman and Omali (2019).

Water facies type

The piper trilinear plot is one of the most useful graphical displays in groundwater quality analyses (Piper, 1944). Compared to other current plotting approaches, it clarifies chemical interactions and improves understanding of the geochemistry of shallow groundwater (Akakuru et al., 2017). Within the anion area, 85% of the total water sample in the area is Cl^- dominant, whereas 10% are HCO_3^- dominant and 5% of the sample had mixed dominant ionic specie. In the cation area, 75% of the total water samples had Ca^{2+} as their dominant ionic specie, while 25% of the samples had mixed dominant ionic specie (Figure 15). According to the Piper diagram, the region is in the geochemical zone 1 (Alkalines earth exceed Akalines). Rocks holding chlorides, agricultural runoff, industrial wastewater, oil well waste, effluent wastewater from wastewater treatment plants, and road salting are a few sources of chlorides that can enter surface water. Metals can

Table 4. Pearson correlation matrix results for the physical and chemical parameters of the groundwater samples.

	pH	Ec	TDS	Ca	Mg	Cl	SO_4	NO_3	DO	K	Na	Fe	HCO_3
pH	1.00												
Ec	-0.11	1.00											
TDS	-0.11	1.00	1.00										
Ca	0.94	-0.10	-0.09	1.00									
Mg	0.69	0.15	0.16	0.78	1.00								
Cl	0.23	-0.39	-0.38	0.39	0.08	1.00							
SO_4	-0.55	0.71	0.71	-0.37	-0.08	-0.24	1.00						
NO_3	-0.16	-0.52	-0.52	-0.05	-0.16	0.19	-0.21	1.00					
DO	-0.64	-0.25	-0.24	-0.39	-0.17	0.31	0.39	0.40	1.00				
K	-0.48	-0.04	-0.04	-0.25	-0.33	0.61	0.43	0.31	0.71	1.00			
Na	-0.24	0.86	0.85	-0.18	0.17	-0.37	0.70	-0.28	-0.02	0.08	1.00		
Fe	0.22	-0.30	-0.30	0.20	0.36	-0.32	-0.31	0.01	0.00	-0.56	-0.08	1.00	
HCO_3	0.86	0.01	0.02	0.93	0.88	0.26	-0.29	0.06	-0.36	-0.26	0.01	0.16	1.00

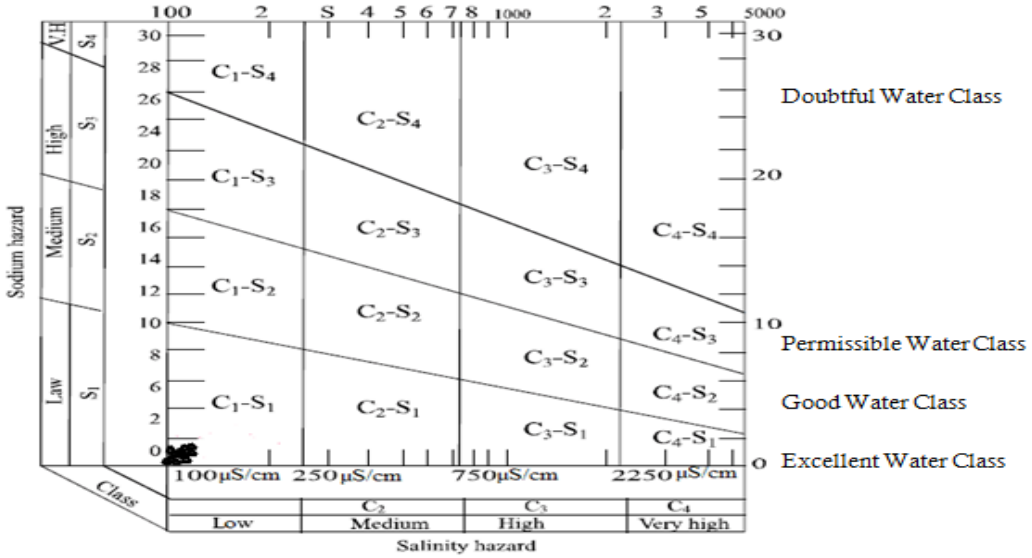

Figure 14. Salinity diagram of the groundwater in the research area.

be corroded by chlorides, and they can also change the flavour of food. Consequently, there is a suggested maximum chloride level for water that is processed for use in industry or any other purpose. Freshwater lakes and streams can become contaminated by chlorides. High quantities of chlorides are toxic to fish and aquatic communities. Due to its buffering properties, calcium serves as a pH stabilizer in addition to being a key factor in water hardness. A nicer taste is also added to water by calcium. Elementary calcium reacts with water at room temperature by the following reaction mechanism, in contrast to magnesium, which is directly above calcium on the periodic table:

$Ca\ (s) + 2H_2O\ (g) \rightarrow Ca(OH)_2\ (aq) + H_2\ (g)$

Calcium hydroxide, which dissolves in water as soda, and hydrogen gas are the products of this process.

Degradation events are additional crucial calcium reaction processes. These typically happen when there is carbon dioxide. Calcium carbonate is normally insoluble in water. Calcium compounds are impacted by the formation of carbonic acid when carbon dioxide is present. The following is the carbon weathering reaction mechanism:

$H_2O+CO_2 \rightarrow H_2CO_3$ and $CaCO_3+H_2CO_3 \rightarrow Ca(HCO_3)_2$

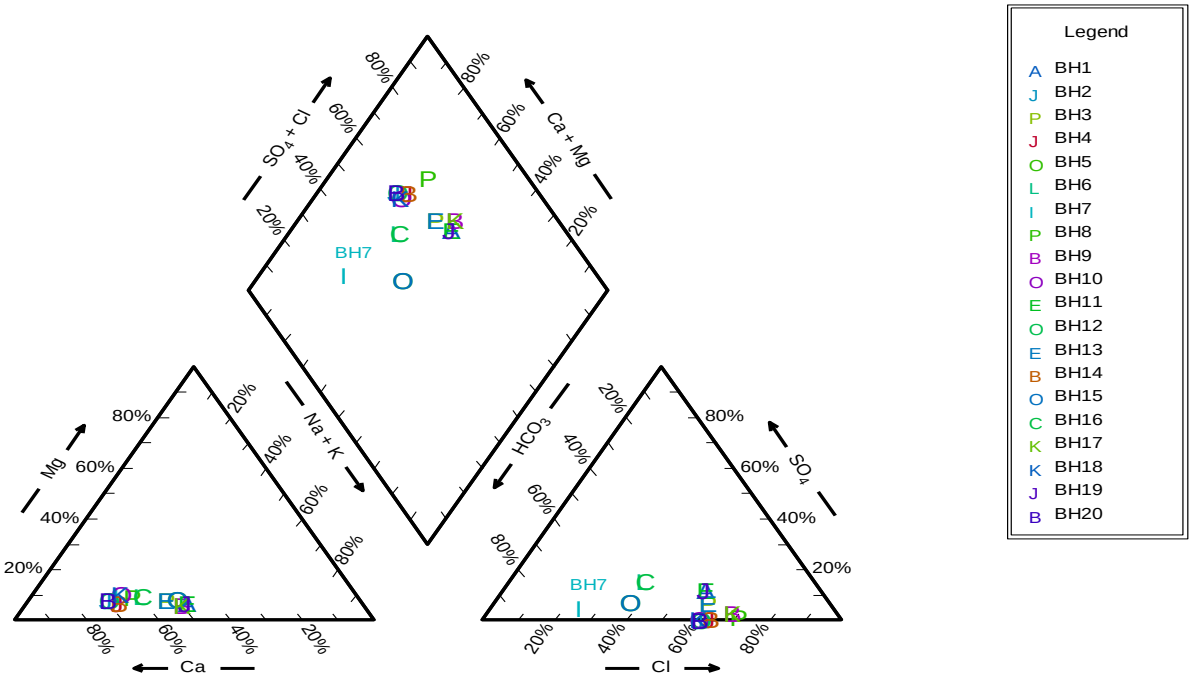

Figure 15. Piper Trilinear plot.

and the total reaction mechanism:

$CaCO_3$ (s) + CO_2 (g) + $2H_2O$ (l) -> Ca^{2+} (aq) + 2 HCO_3^- (aq)

The product is calcium hydrogen carbonate.

Many academics have utilized Durov diagram to characterize the hydrogeochemical composition of groundwater. Its effectiveness has long been recognized. The Durov plot in Figure 16 demonstrates how similar the Durov is to the Piper diagram. It also demonstrates that there is ionic exchange occurring within the groundwater zone. This research agrees with that of Nigerian researchers Anudu et al. (2008); Akakuru et al. (2022) and Piper (1944). Schoeller semi-logarithmic plot (Akakuru et al., 2023; Iheme et al., 2018a) in the study area shows the hydrogeochemical evolution trend of Cl^-> HCO_3^-+CO_3^{2-}> Ca^{2+}>Na^++K^+> SO_4^{2-}> Mg^{2+}. The dominance of Cl^- in the research area could be from man-made or natural sources. Ca^{2+} source could be attributed to dissolved rock minerals containing Ca^{2+}, particularly from, dolomite, limestone and gypsum (Cheng et al., 2016; Akakuru et al., 2017).

Multivariate statistics

The correlation matrix and the Principal Component Analysis were utilized for this study. In the present study, the Pearson correlation analysis results (Table 4) reveal a strong correlation between $_P$H and Ca, Mg, SO_4, DO, K, HCO_3; Ec and SO_4, NO_3; TDS and SO_4, NO_3, Na; Ca and Mg, HCO_3; Mg and HCO_3; Cl and K, SO_4 and Na; NO_3 and DO; DO and K; K and Fe. This strong correlation detected from the result proposes the likelihood of similar sources of enrichment for the parameters. Hence, this implies that the indicators emanated from common natural or anthropogenic sources. These results compare favourably with the results of Anizoba et al. (2015); Gopinath et al. (2018) and Yuan et al. (2014).

Principal component analysis

The PCA is an essential tool for identifying designs, analyzing the variation of networks of connected components, and further isolating the Eigenvalues and Eigenvectors (loadings) for head parts from the change that they are subject to (Yuan et al., 2014). It illustrates the relationship between the factors to pinpoint the most likely sources of groundwater contamination in the review area. There were found to be three important principal components. In the analysis interpretation, every loading that is more than 0.4 (+ or -) is regarded as having been a substantial contributor (Akakuru et al., 2022). According to Table 5, loadings were present for 37.42% of the parameters in PP1, 65.60% of the parameters in PP2, in

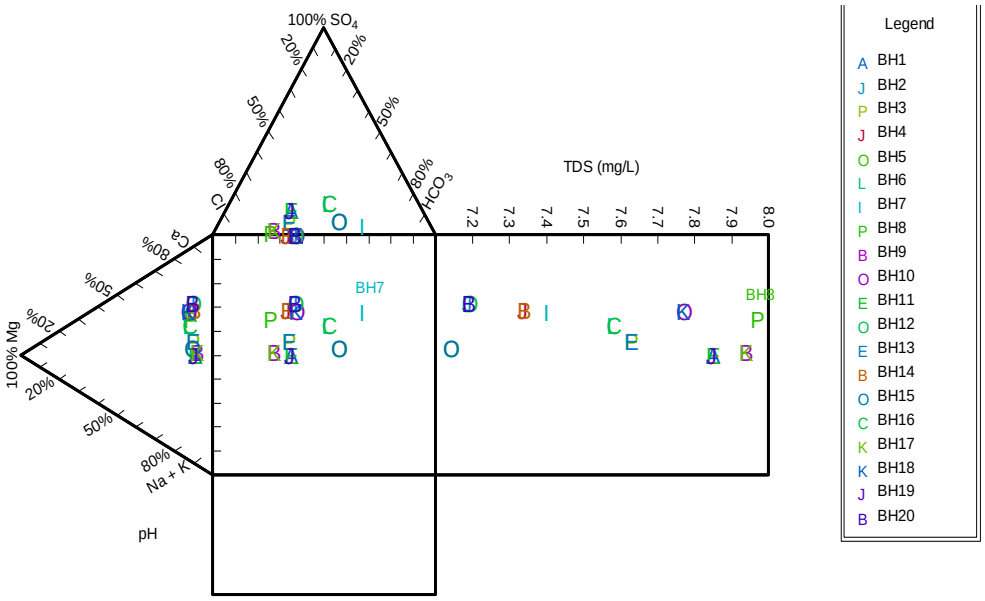

Figure 16. Durov plot.

PP3, it had 75.23 loadings. The findings of this PCA suggest that loadings within the groundwater system may have resulted from anthropogenic activities in the area that are changing the chemistry of the water.

Suitability of the groundwater for irrigation purposes

Five irrigation suitability parameters were calculated to ascertain the fitness of the groundwater sources for irrigation purposes:

Sodium Absorption Ration (SAR)

The salt content of water is crucial for irrigation since it influences plant growth. In the presence of carbonate and salt, alkaline soils will develop. Saline soil is created when salt and chloride are combined (Akakuru et al., 2023). Similar to this, sodium is absorbed by clay surfaces to produce alkaline earth minerals.

By altering the soil's structure, which makes it compact and impermeable and considerably slows down plant growth, this is accomplished (Yuan et al., 2014; Zhu et al., 2019). The various cycles, including ionic trade responses in soil, must be made clear by SAR. In the study, SAR values (meq/L) from groundwater range between 1.49 and 4.16, with a mean of 2.58 and a standard deviation of 0.90 (Table 6) while Figure 17 is the Boxplot showcasing how the SAR values in the data are spread out. It is rated as excellent for irrigation in the research area based on the SAR data (Emmanuel and Nurudeen, 2012; Omali et al., 2018a). The findings of Iheme et al. (2018a, b) and Omali et al. (2018b) in their independent groundwater contemplates in South Africa, Nigeria, and Tunisia, respectively, are consistent with this result.

Percentage sodium (%Na^+)

The increase in %Na^+ is deemed unsuitable for the water system but demonstrates a cation exchange with magnesium and calcium in the soil (Aikpokpodion et al., 2010). The waste and porosity of the dirt are reduced by this trade. In dry conditions, the dirt is somewhat extreme, and dampness on the dirt reduces air and water dissemination (Akakuru et al., 2017; Todd, 1980). Alkaline soils are created when sodium chloride is present in the presence of inorganic carbon, and these soils eventually turn saline. These types of soil are not suited for plant growth (Anudu et al., 2008). Therefore, a key factor in establishing whether groundwater is suitable for irrigation is the sodium content of agricultural products. With a mean of 41.32 and a standard deviation of 10.17, the percent Na^+ values (percent) in Table 6 range from 29.55 to 55.17. The boxplot in Figure 18 shows how the percent Na values in the data are distributed. Since the overall sample meets the criterion for groundwater quality and is less than 20, the groundwater in the research region is suitable for irrigation. This result confirms the SAR finding that all of the measured groundwater is very suitable for irrigation.

The outcome is consistent with and comparable to

Table 5. PCA values.

Parameter	Communalities	Components		
		1	2	3
pH	0.96	0.91	0.33	0.13
Ec	0.98	-0.47	0.86	0.14
TDS	0.97	-0.46	0.86	0.14
Ca	0.96	0.85	0.29	0.39
Mg	0.76	0.63	0.52	0.32
Cl	0.82	0.27	-0.44	0.74
SO_4	0.84	-0.76	0.40	0.32
NO_3	0.42	0.08	-0.62	0.17
DO	0.64	-0.45	-0.54	0.38
K	0.96	-0.50	-0.43	0.73
Na	0.80	-0.50	0.72	0.16
Fe	0.42	0.42	0.02	-0.49
HCO_3	0.94	0.78	0.38	0.42
	Eigenvalues	0.79	2.35	3.56
	Variance (%)	37.42	28.21	9.60
	Cumulative var. (%)	37.42	65.63	75.23

Table 6. Irrigation parameter values for individual samples.

Parameter	SAR	%Na	MH	KR	SSP
BH1	3.74	54.79	9.09	0.73	54.79
BH2	1.49	29.55	7.32	0.26	29.55
BH3	2.92	48.24	9.09	0.57	48.24
BH4	2.01	32.94	6.67	0.34	32.94
BH5	4.16	46.84	10.34	0.86	46.84
BH6	2.55	37.25	9.68	0.51	37.25
BH7	2.47	30.47	9.28	0.4	30.47
BH8	1.71	37.74	9.09	0.33	37.74
BH9	2.33	55.17	7.69	0.59	55.17
BH10	1.9	32.12	9.68	0.31	32.12
BH11	3.74	54.79	9.09	0.73	54.79
BH12	1.49	29.55	7.32	0.26	29.55
BH13	2.92	48.24	9.09	0.57	48.24
BH14	2.01	32.94	6.67	0.34	32.94
BH15	4.16	46.84	10.34	0.86	46.84
BH16	2.55	37.25	9.68	0.51	37.25
BH17	2.33	55.17	7.69	0.59	55.17
BH18	1.9	32.12	9.68	0.31	32.12
BH19	3.74	54.79	9.09	0.73	54.79
BH20	1.49	29.55	7.32	0.26	29.55
Mean	2.58	41.32	8.69	0.5	41.32
Min	1.49	29.55	6.67	0.26	29.55
Max	4.16	55.17	10.34	0.86	55.17
Stdv	0.9	10.19	1.18	0.2	10.19

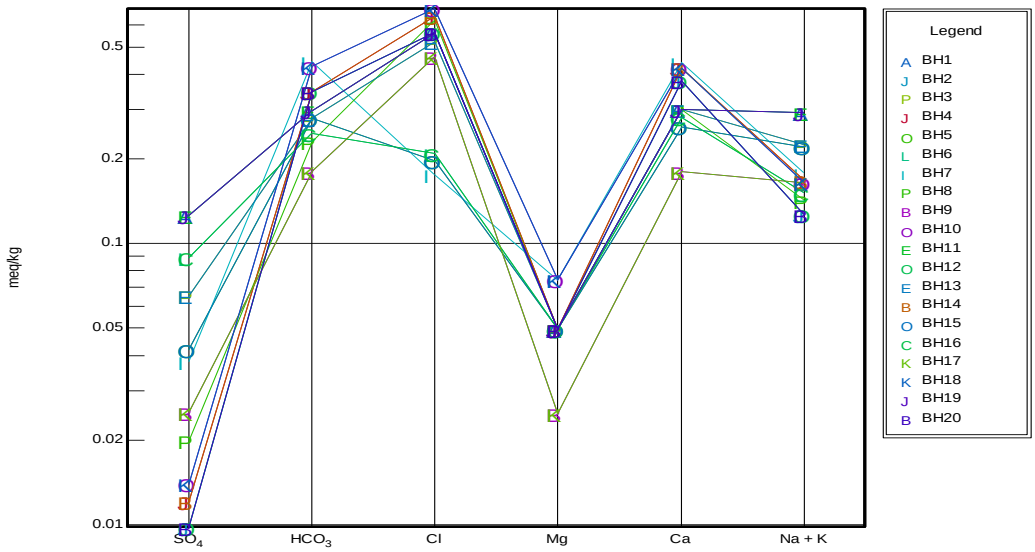

Figure 17. Schoeller semi-logarithmic plot of the ionic trend in the research area.

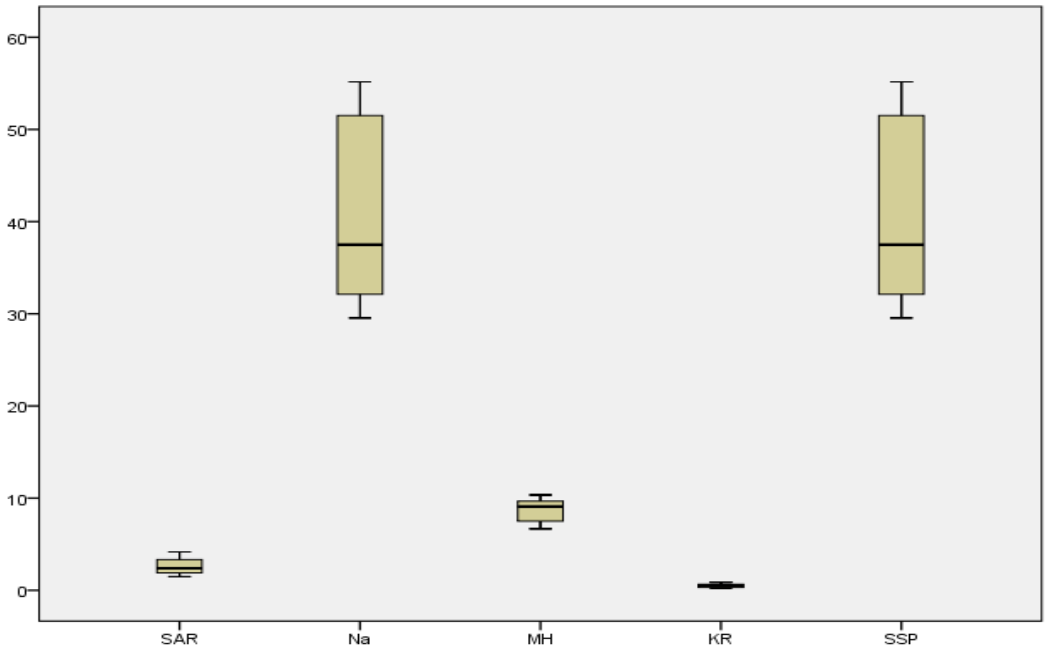

Figure 18. Boxplot showing the irrigation parameters.

previous research from China, Italy, Pakistan, and India by Buckley et al. (1995), Chetelat et al. (2008) and Yuan et al. (2014).

Magnesium hazard

When determining the water reasonableness limit for water system purposes, the risk of magnesium is a key factor. Too much magnesium in the water causes pungency, which slows down plant growth and productivity (Akakuru et al., 2017).

An MH proportion of greater than 50 is deemed unacceptable, hazardous, or inappropriate for use in the water supply. However, an MH convergence of 50 is deemed suitable for a water system (Akakuru et al.,

2023; Egboka, 1986). The MH values varied from 6.67 to 10.34, according to Table 6, with a mean of 8.69 and a standard deviation of 1.18, while Figure 18 the Boxplot shows how the MH values are distributed across the data. As a result, 100% of the samples had a minimum age of 50, indicating that they are suitable for use in water systems. This result is consistent with studies conducted by Richards (1954), Udoh et al. (2021), Zhu et al. (2019) in China, and Akakuru et al. in Nigeria in 2022. However, it does not align with research conducted in China (Yuan et al., 2014).

Kelly's ratio

Based on its effectiveness in determining the appropriateness of groundwater for irrigation, KR has been a genuine instrument (Akakuru et al., 2017). Any result below one is good for irrigation, whereas any value above one indicates that the amount of Na in the groundwater is high. With a mean of 0.50 and a standard deviation of 0.26, Table 6 reveals that KR values vary from 0.26 to 0.86, while Figure 18 is a boxplot illustrating how the KR values in the data are distributed. Additionally, this outcome demonstrates that the entire sample of groundwater is acceptable for irrigation. The outcome supports the conclusions reached by other irrigation assessment methods, all of which concur that the water is acceptable for irrigation. This finding is in line with those of Emmanuel and Nurudeen (2012) in India and Azuoko et al. (2023) in Nigeria. But this result runs counter to what Akakuru et al. (2022) found in South Africa.

Soluble Sodium Percentage (SSP)

SSP has been utilized by scholars in the assessment of the suitability of groundwater for irrigation purposes. It assesses the percentage of soluble sodium in groundwater. SSP less than 50 is suitable for irrigation, while above 50 is considered unsuitable. The result from Table 6 shows that SSP values range between 29.55 and 55.17 with a mean of 41.32 and a standard deviation of 10.19 while Figure 18 is the Boxplot showcasing how the SSP values in the data are spread out. The result shows that 75% of the samples are safe and suitable for irrigation, while 25% are not. SSP aligns with other irrigation assessment tools. This result is in agreement with the work of Akakuru et al. (2023) done in the Niger Delta Nigeria.

Conclusion

The researched area is characterized by curves H-type, AK-type, KH-type, KHK-type, QQ-type, KQQ-type, KQ-type, HK-type, HKH-type, KHA-type and AKH-type. It is observed that the AK-type curve predominates the study area especially areas overlain by Ajali Formation. The interpretative cross-section of AA1 shows three to five geoelectric units. The top-most unit is characterized by resistivity values ranging from 174 to 718 Ω.m with thickness that varies from 0.6m to 8.9m and is composed of predominantly top sandy soil. The second unit has resistivity values that vary from 9.2 to 5310 Ω.m contains silty shale in VES 3 and sand in other VES locations. The third unit with resistivity range of 13.1 to 718 Ω.m and a thickness between 12.8 and 66.1 m. The base layer bottom was not reached and it has a resistivity value ranging from 15.1 to 1980 Ω.m. It was interpreted as shale. Again, the correlation along BB1 in the NW-SE direction (Figure 10) shows the high thickness of topsoil at VES 10. The deepest depth to a saturated unit within this region is at VES 18 (Amokwe Amaba), whereas VES 6, 9 and 10 have shallower saturated units. Mostly, the auriferous zone is continuous with numerous facie changes within the research area and can produce an optimum amount of water.

The resistivity map of the study area reveals high resistivity towards the Northwest, Southeast and Southern parts of the research area. Also, the 2-D and 3-D water-table depth maps reveal a higher concentration of contour lines towards the Southern part of the research area. Hence, the water-table depth maps revealed a high hydraulic gradient towards the Southern part of the researched area. It can be concluded from the research that the VES method can be used not only for groundwater exploration but also contributes to the identification of various geologic units. This study has revealed different subsurface layers, and the nature of groundwater quality in the Isuikwuato area From the physicochemical analysis, most of the physical and chemical parameters of the groundwater in the research area fall within WHO (2006) guidelines for drinking water and the analytical data plotted on the Salinity diagram (Baba et al., 2018; Chinwuko et al., 2016; Short and Stauble, 1967) template depicts that all the groundwater samples are within the field of C1S1 (under low salinity and low Na hazard), indicating that the samples are within the excellent class.

The hydrogeochemical characterization of the study area is the anion area, 85% of the total water sample in the area is Cl^- dominant, whereas 10% are HCO3- dominant and 5% of the sample had mixed dominant ionic specie. In the cation area, 75% of the total water samples had Ca^{2+} as their dominant ionic specie, while 25% of the samples had mixed dominant ionic specie. According to the Piper diagram, the region is in the geochemical zone 1 (Alkalines earth exceeds Akalines). The Durov plot also demonstrates that there is ionic exchange occurring within the groundwater zone with a

hydrogeochemical evolution trend of Cl-> HCO_3-+CO_3^{2}-> Ca^{2+}>Na^{+}+K+> SO_4^{2}> Mg^{2+}. This strong correlation observed within parameters detected from the result proposes the likelihood of similar sources of enrichment for the parameters. PCA values indicated loadings were present for 37.42% of the parameters (PP) in PP1, 65.60% of the parameters in PP2, and in PP3, it had 75.23 loadings. The irrigation suitability of the groundwater in the area showed that the water is suitable for agriculture based on SAR, %Na, MH, KR, and SSP results. This study, therefore, suggests or recommends that the government should leverage this to the availability of clean water and food to the people to enable it to achieve its food agriculture and clean water policies in tandem with the sustainable development goals (SDGs).

CONFLICT OF INTERESTS

The authors have not declared any conflict of interests.

ACKNOWLEDGEMENTS

The authors extend their sincere gratitude to Prof. Izuchukwu Obiadi, Department Head of Nnamdi Azikiwe University's Applied Geophysics Department, for granting us permission to utilize their equipment for conducting the geophysical survey. Additionally, they appreciate Kogi State University's Department of Earth Sciences forgranting them access to their laboratory for conducting the geochemical analysis.

REFERENCES

Adetola BA, Igbedi AO (2000). The use of electrical resistivity survey in location of aquifers: a case study in Agbede South Western Nigeria. Journal of Nigerian Association of Hydro-geologists 11(5):7-13.

Aikpokpodion PE, Lajide L, Aiyesanmi AF (2010). Heavy Metals Contamination in Fungicide Treated Cocoa Plantations in Cross River State, Nigeria. American-Eurasian. American-Eurasian Journal Agric. & Environ. Science 8(3):268-274.

Akakuru OC, Akudinobi BEB, Usman AO (2017). Organic and Heavy Metal Assessment of Groundwater Sources Around Nigeria National Petroleum Cooperation Oil Depot Aba, South-Eastern, Nigeria. Journal of Natural Sciences Research 7(24):48-54.

Akakuru OC, Eze CU, Okeke OC, Opara AI, Usman AO, Iheme OK, Ibeneme SI, Iwuoha PO (2022). Hydrogeochemical evolution, water quality indices, irrigation suitability and pollution index of groundwater (PIG) around Eastern Niger Delta, Nigeria. International Journal of Energy and Water Res
ources. https:doi.org/10.1007/s42108-021-00162-0

Akakuru OC, Chidi BA, Ikoro DO, Eyankware MO, Opara AI, Njoku AO, Iheme AO, Usman AO (2023). Application of Artificial neural network and multi-linear Regression Techniques in Groundwater Quality and Health Risk Assessment around Egbema, Southeastern Nigeria. Environmental Earth Sciences 82:77 http://dx.doi.org/10.1007/s12665-023-10753-1

Anizoba DC, Chukwuma GO, Chukwuma EC, Chinwuko AI (2015). Determination of aquifer characteristics from geoelectrical sounding data in parts of Anambra State, Nigeria. International Journal of Innovation and Applied Studies 11(4):832-843.

Anudu GK, Obrike SE, Onuba LN (2008). Physicochemical quality of groundwater in Abagana and its environs, Anambra Basin, southeastern Nigeria. International Journal of Chemical Sciences 1(2):296-301.

Azuoko GB, Nwanekezi-Phil CG, Usman AO (2023). Assessment of Near Surface Corrosivity and Competence within Alex Ekwueme Federal University and Environs, Southeastern Nigeria Using Electrical Resistivity Method. FUNAI Journal of Science and Technology 6(1):58-70.

Baba Y, Omali AO, Usman AO (2018). Geochemical and Geophysical Investigations of Kaolin Deposits of the Maastrichtian Mamu Formation, Northern Anambra Basin, Nigeria. International Journal of Geophysics and Geochemistry 5(2):45-52.

Bobachev A (2002). IPI2win- a window software of an automatic interpretation of resistivity sounding data. PhD Thesis, Moscow State University 55:1-78.

Buckley NA, Dawson AH, Reith DA (1995). Controlled release in overdose: clinical considerations. Drug Safety 12(1):73-84.

Chetelat B, Liu CQ, Zhao ZQ, Wang QL, Li S, Li J, Wang BL (2008). Geochemistry of the dissolved load of the Changing Basin Rivers: Anthropogenic impacts and chemical weathering. Geochemical and Cosmochemical 72(3):4254-4277.

Chukwu GU (2008). Water quality Assessment of Boreholes in Umuahia South Local Government Area of Abia State. The Pacific Journal of Science and Technology 9(2):592-594.

Chinwuko AI, Anakwuba EK, Okeke HC, Onyekwelu CU, Usman AO, Osele CE, Iheme OK (2016). Assessment of Hydrogeophysical and Geotechnical Properties in Central Part of Anambra State, Nigeria. International Journal of Geophysics and Geochemistry 3(2):6-13.

Chinwuko AI, Anakwuba EK., Okeke HC, Usman AO, Ovwasa MO, Okoye IF (2015). Geo-electric Investigation for Groundwater Potential in Awka Anambra State, Nigeria. International Journal of Science for Global Sustainability 1(1):85-95.

Davis SN, Deweist RJM (1966). Hydrogeology. John Wiley and Sons, Inc. 463 p.

Egboka BCE (1986). Hydrogeochemistry of shallow wells and surfacewaters of Owerri and its environs. production. 1st Symposium of Nigerian Inland Water and Safety Agency 2(1):305-328.

Emmanuel B, Nurudeen A (2012). Physiochemical analysis of groundwater samples in Bichi local government of Kano state, Nigeria. Journal of Science and Technology 2(2):2225-7217.

Ezeh CC, Oti UA, Usman AO, Okonkwo AC (2022). 2-Dimensional Resistivity Imaging of Inyi Coal-Field, Anambra Basin, Nigeria. Journal La Multiapp 2(6):40-54.

Gopinath S, Srinivasamoorthy K, Saravanan K, Prakash (2018). Discriminating groundwater salinization processes in coastal aquifers of southeastern India: geophysical, hydrogeochemical and numerical modeling approach. Environmental Development Sustainability 3(1):54-88.

Gopinath S, Srinivasamoorthy K, Saravanan K, Suma CS, Prakash R, Senthilnathan D (2016). Modeling saline water intrusion in Nagapattinam coastal aquifers, Tamilnadu, India. Modeling Earth Systems and Environment 5(3):66-99.

Iheme KO, Akudinobi BEB, Oyeleke TA, Ibrahim KO, Abubakar HT, Usman AO (2018a). An Evaluation of Groundwater and Surface Water Resources in Orlu and Environs, South Eastern Nigeria. Journal of Basic Physical Research 8(2):31-38.

Iheme KO, Usman AO, Obaro RI, Aganigbo CI, Gbadebo AF (2018b). Hydro-Geophysical Assessment of Groundwater Resources within parts of Omu Aran, South Western Nigeria. USEP: Journal of Research Information in Civil Engineering 15(4):2393-2417.

Obi GC, Okogbue CO, Nwajide CS (2001). Evolution of the Enugu Cuesta: A tectonically driven erosional process. Global Journal of Pure and Applied Sciences 7:321-330.

Omali AO, Usman AO, Baba Y (2020). Evaluation of Groundwater resources within Ankpa and Environ, North-Centre Kogi State. International Journal of Advance Geosciences 8(1):65-74.

Omali AO, Egboka BCE, Usman AO (2018a). Seasonal variations in the

Physico-Chemical and Microbial Characterization of Groundwater in Lokoja North Central Nigeria. Journal of Basic Physical Research 8(2):117-134.
Omali AO, Usman AO, Oguche II (2018b). Hydrogeophysical Evaluation of Groundwater Resources within some parts of Northern Anambra Basin, Nigeria. Journal of Earth Sciences and Geotechnical Engineering 8(4):17-33.
Piper AM (1944). A graphical presentation in geochemical interpretation of water analysis. Transaction American Geophysics Union 25:914-923.
Reyment RA (1965). Aspects of the Geology of Nigeria. University of Ibadan Press, Nigeria P 145.
Richards LA (1954). Diagenesis and improvement of saline alkali soils. Agric Handbooks 60, U.S Department Agriculture Washington D.C 160 p.
Selemo AOI, Okeke PO, Nwankwo GI (1995). An appraisal of the usefulness of vertical electrical sounding (VES) in groundwater exploration in Nigeria. Water Resources 6(1-2):61-67.
Short KC, Stauble AJ (1967). Outline of geology of Niger delta. American Association of Petroleum Geologists Bulletin 51:761-779.
Todd DK (1980). Groundwater Hydrology. John Wiley and Sons, New York, 2nd edition 524 p.
Udoh AC, Chinwuko AI, Onwuemesi AG, Anakwuba EK, Oyonga AO, Usman AO (2021). Impact of Solid Waste on Groundwater Quality in Selected dumpsites in Awka Ibom State, Nigeria Using Resistivity and Hydrochemical Data. Bulletin of the Mineral Research and Exploration. 164:231-246. https://doi.org/10.19111/bulletinofmre.753240
Usman AO, Iheme KO, Chinwuko AI, Azuoko GB, Akakuru OC (2022). Hydro-Geophysical investigation of Groundwater Resources within Abakaliki, lower Benue Trough, Nigeria. COOU Journal of Physical Science 5(1):471-491.
Usman AO, Omali AO (2019). Geophysical and Geochemical assessment of Groundwater within parts of Kogi East Northern Anambra Basin, Nigeria. Development Journal of Science and Technology Research 8(1):46-63.
Usman AO, OmadA JI, Omali AO, Akakuru OC (2015). Evaluation of the Aquifer characteristics of Nteje and Environs, Anambra Basin, South Eastern Nigeria. Journal of Natural Science Research 5(14):99-115.
World Health organization (WHO)/ United Nations Environmental Program (UNEP)/ United Nations Education Scientific and Cultural Organization (UNESCO)/ World Meteorological Organization (WMO) (1998). Global Environmental Monitoring System/Water Operational Guide.
World Health Organization (WHO) (2006). Guidelines for drinking water quality criteria, 2nd Edition, 2, 281-308 World Health Organization, Geneva.
Yuan J, Mao X, Wang Y, Deng Z, Huang L (2014). Geochemistry of rare-earth elements in shallow groundwater, northeastern Guangdong Province, China. Chinese Journal of Geochemistry 33:53-64.
Zhu HY, Wu LJ, Xin CL, Yu S, Guo YS, Wang JJ (2019). Impact of anthropogenic sulfate deposition via precipitation on carbonate weathering in a typical industrial city in a karst basin of southwest China: a case study in Liuzhou. Applied Geochemistry 110:104417.